J. Ocean Univ. China (Oceanic and Coastal Sea Research)
https://doi.org/10.1007/s11802-018-3467-0
ISSN 1672-5182, 2018 17 (3): 487-497
http://www.ouc.edu.cn/xbywb/
E-mail:xbywb@ouc.edu.cn

Analysis of Dynamic Characteristics of the 21st Century Maritime Silk Road

ZHANG Xudong[1), 2)], ZHANG Jie[2)], FAN Chenqing[2)], MENG Junmin[2)], WANG Jing[1)], and WAN Yong[3), *]

1) *College of Information Science and Engineering*, *Ocean University of China*, *Qingdao* 266100, *China*
2) *First Institute of Oceanography*, *State Oceanic Administration*, *Qingdao* 266061, *China*
3) *College of Information and Control Engineering in China University of Petroleum*, *Qingdao* 266580, *China*

(Received March 8, 2017; revised April 13, 2017; accepted December 15, 2017)

Abstract The 21st century Maritime Silk Road (MSR) proposed by China strongly promotes the maritime industry. In this paper, we use wind and ocean wave datasets from 1979 to 2014 to analyze the spatial and temporal distributions of the wind speed, significant wave height (SWH), mean wave direction (MWD), and mean wave period (MWP) in the MSR. The analysis results indicate that the Luzon Strait and Gulf of Aden have the most obvious seasonal variations and that the central Indian Ocean is relatively stable. We analyzed the distributions of the maximum wind speed and SWH in the MSR over this 36-year period. The results show that the distribution of the monthly average frequency for SWH exceeds 4 m (huge waves) and that of the corresponding wind speed exceeds 13.9 $m\,s^{-1}$ (high wind speed). The occurrence frequencies of huge waves and high winds in regions east of the Gulf of Aden are as high as 56% and 80%, respectively. We also assessed the wave and wind energies in different seasons. Based on our analyses, we propose a risk factor (RF) for determining navigation safety levels, based on the wind speed and SWH. We determine the spatial and temporal RF distributions for different seasons and analyze the corresponding impact on four major sea routes. Finally, we determine the spatial distribution of tropical cyclones from 2000 to 2015 and analyze the corresponding impact on the four sea routes. The analysis of the dynamic characteristics of the MSR provides references for ship navigation as well as ocean engineering.

Key words Maritime Silk Road; risk factor; ocean wave; wind speed; tropical cyclone

1 Introduction

The ocean is the common natural bond supporting the interaction of different economies and cultures. The North Indian Ocean and South China Sea (SCS) have many sea routes that connect major economic blocks, such as the Association of Southeast Asian Nations, South Asia, North Africa, and Europe. The 21st century Maritime Silk Road (MSR) proposed by China, which includes the North Indian Ocean and SCS, plays an important role in the communication between different economic cultures and strongly promotes navigation activities (Zheng *et al*., 2015). The MSR also overlaps with other important routes in the busy shipping regions of the SCS and North Indian Ocean. Hence, an analysis of the dynamic characteristics of the MSR can promote safe ship navigation and provide vital references for ocean engineering.

The SCS and Indian Ocean are renowned global monsoon areas that have been the focus of much research by many scholars (Chu and Cheng, 2008; Sabique *et al*., 2013; Bhat and Fernando, 2016; Liu *et al*., 2016; Luo *et al*., 2016). Jignesh *et al*. (2001) derived wind speed and wave parameters from TOPEX/POSEIDON altimetry data and compared the results with ocean buoy data from the North Indian Ocean. Qi and Cao (2016) investigated SWHs in the North Indian Ocean with Jason-2 altimetry data. Mei *et al*. (2010) applied the WAVEWATCH-3 (WW3) model to study the wave field and used the empirical orthogonal function to study the wind field of the SCS and North Indian Ocean. The authors found that the high SWH in the central Indian Ocean may be explained by the northward swell generated in the southern Indian Ocean by westerly winds. Sabique *et al*. (2012) studied the swell propagation from the southern Indian Ocean based on a third-generation wave model and accounted for its contribution to the local wave climate in the North Indian Ocean. Not only the wave model and remote sensing data could be applied to analyze the wind and wave fields, the reanalysis data can also provide a long term dataset for the investigation. Semedo *et al*. (2011) used the ERA-40 dataset to analyze global wave and wind fields and also calculated the energy of the ocean wave field. Liu *et al*. (2013) analyzed the long-term linear trend of the sea surface wind speed from 1958 to 2001 in the North Indian Ocean. Lv *et al*. (2014) applied the Simulating Waves

* Corresponding author. E-mail: wanyong@upc.edu.cn

Nearshore model driven by wind data from the European Center for Medium-Range Weather Forecasts (ECMWF) to investigate the wave characteristics in the Bohai Sea from 1993 to 2012. Shanas and Sanil (2014) and Anoop *et al*. (2015) analyzed the ERA-interim reanalysis data to investigate the wave and wind fields in the eastern Arabian Sea and Indian Ocean.

Extreme weather conditions, such as the tropical cyclones, pose a severe threat to ships. Many scholars have conducted research on extreme weather conditions (Murakami *et al*., 2012; Werner *et al*., 2012; Rajasree *et al*., 2016). Yuan *et al*. (2007) studied the characteristic differences of tropical cyclones in the western North Pacific and the SCS. Ho *et al*. (2006) examined the variation of tropical cyclone activity in the south Indian Ocean for the 1979 to 2004 period and analyzed the impact of the El Niño–Southern Oscillation and the Madden-Julian Oscillation on these variations. Wang *et al*. (2009) studied the influence of tropical cyclones on the seasonal variability of ocean circulation in the SCS. Ng *et al*. (2012) analyzed the inter-annual variations of tropical cyclone activity over the North Indian Ocean from 1983 to 2008 and presented the tropical cyclone tracks. Rajasree *et al*. (2016) conducted a comparative study of tropical cyclones in the North Indian and Atlantic Oceans. Despite the extensive investigations of the properties of tropical cyclones by many scholars and the advances in our understanding, little attention has been paid to the effect of these properties on maritime navigation.

Although much research has also been conducted on the waves and wind in the SCS and Indian Ocean, further detailed analyses of their effects on maritime navigation is required. In this paper, we analyze the seasonal distribution of ocean waves and wind and examine the monthly averages of high winds and huge waves from 1979 to 2014. We also consider the wave and wind energies of different seasons to provide references for ocean engineering. We calculate the temporal and spatial distributions of the corresponding risk factor (RF) to determine navigation safety levels. We also determine the spatial distribution of tropical cyclones from 2000 to 2015 and briefly analyze the corresponding effects on sea routes.

The rest of this paper is organized as follows: In Section 2, we present our data and validation. In Section 3, we present the spatial and temporal distributions of the dynamic ocean characteristics. In Section 4, we present our analyses of the monthly average distributions of huge waves and high winds, briefly assess the wave and wind energies, and discuss the impact of huge waves, high wind speeds, and tropical cyclones on major sea routes. In Section 5, we summarize our findings.

2 Material and Methods

ERA-Interim is a reanalysis of the global atmosphere that covers the data-rich period from 1979 and continuing in real time. Global wave field data can be obtained from ERA-Interim, including the significant wave height (SWH), mean wave direction (MWD), and mean wave period (MWP) of ocean waves. With the support of the Special Fund for Marine Renewable Energy project, a buoy was placed in the SCS, as shown in Fig.1, and the SWH and wave period were measured during the project. Table 1 lists the specifications of the buoy.

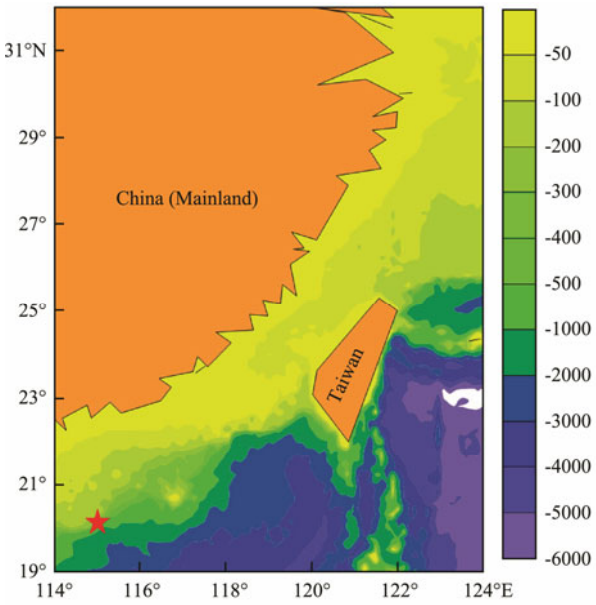

Fig.1 Topographic map of East Sea and SCS. The red star indicates the position of the buoy.

Table 1 Buoys data specifications

Buoy ID	Location or range	Water depth (m)	Data period	Time interval	General location
Buoy_PY30-1	20.2447°N, 114.9413°E	240	Mar. 2012 to Jul. 2012	1 h	South China Sea

Fig.2 shows a comparison of the SWH from the ERA-Interim and the Buoy_PY30-1. As shown in the figure, the number of samples collocated with Buoy_ PY30-1 is 2883, the root mean square error (RMSE) is 0.36 m, and the correlation coefficient (CC) is 0.95. For the comparison of the mean wave periods, the number of samples collocated with Buoy_PY30-1 is 2652, the RMSE is 0.76 s, and the CC is 0.78.

The results show that the dataset from the ERA-Interim are sufficiently accurate for use in our study. Based on 36-year reanalysis data from 1979 to 2014, we determined the spatial and temporal distributions of ocean waves and wind speed. We obtained the monthly, seasonal, and annual averages from the averages of the 36-year data for every location in the study area, which comprised the region 17°S–30°N, 33°–122°E. The spatial resolution of the dataset is 0.125° and the temporal resolution is 6 h.

First, we determined the distribution of the wave and wind energies in the study area. We calculated the rela-

tionship of the wave energy to the SWH and MWP as follows (Zheng *et al*., 2013):

$$Pw = \frac{\rho g^2}{64\pi} \cdot SWH^2 \cdot MWP \approx 0.5 \cdot SWH^2 \cdot MWP .$$

We calculated the relationship of the wind energy to the wind speed (V) and air density (ρ) as follows:

$$W = 0.5 \cdot \rho \cdot V^3 .$$

The International Best Track Archive for Climate Stewardship (IBTrACS) provides best-track data for tropical cyclones. IBTrACS works directly with all the Regional Specialized Meteorological Centers and other international centers and individuals to create a global best-track dataset that contains the most complete historical global set of historical tropical cyclones available. In this paper, we used IBTrACS Version v03r08 to extract the best tracks of tropical cyclones from 2000 to 2015.

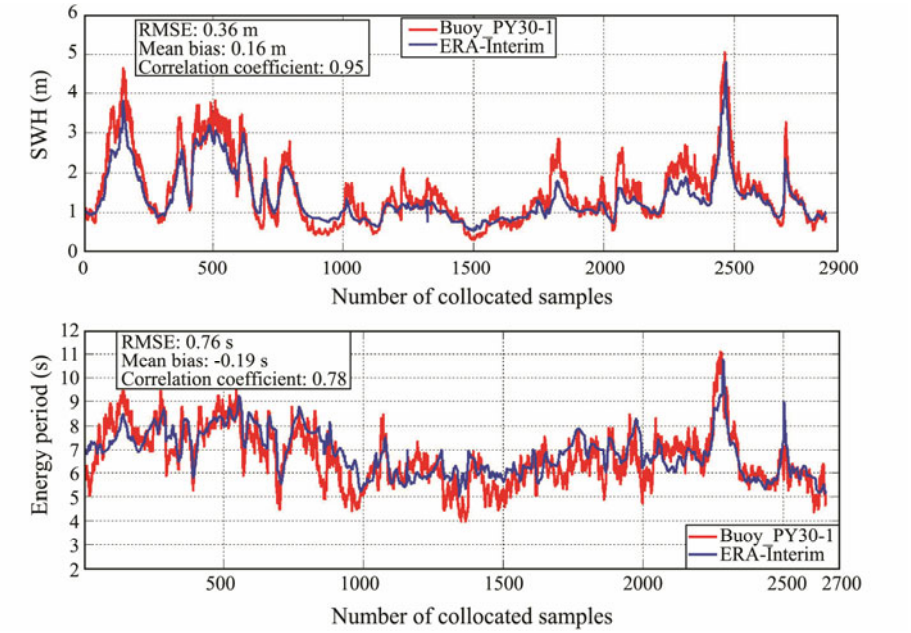

Fig.2 Plots of SWH and energy period from Buoy_PY30-1 (top) *versus* data extracted from ECMWF (bottom).

3 Results

The SWH, MWD, and MWP are important parameters with respect to ocean waves. Together with wind speed, these parameters are crucial considerations for the safe navigation of ships. We applied the 36-year ECMWF data to analyze these parameters in the study area. In this paper, we defined the seasons in terms of the Northern Hemisphere, whereby spring comprises March, April and May; summer is June, July and August; autumn is September, October, and November; and winter is December, January, and February.

3.1 Distributions of the SWH and MWD

The distributions of the SWH and MWD show obvious seasonal variations due to the effect of monsoon. Fig.3 presents the seasonal-average distributions of the SWH and MWD. We can see that in every season, the highest SWH is located in the central Indian Ocean. East of the Gulf of Aden shows obvious seasonal variations, with the SWH being highest in summer and lowest in spring. Affected by the doldrums, the SWH shows a latitudinal zonal distribution with a low value along the equator, especially in the regions between 50°–70°E. In addition to the influence of the local monsoon, the swell originating from the Southern Ocean also plays a non-negligible role for the high SWH in the central Indian Ocean (Semedo *et al*., 2011). This effect can also be observed in the wave direction in every season. The waves mainly propagate from south to north in the central Indian Ocean. The SWH in the SCS also shows seasonal variation due to the influence of monsoon. Under the influence of a strong northeast monsoon, the SWH in the SCS is highest in winter, up to 2.4 m. In spring, the northeast monsoon gradually weakens, which leads to a decrease in the SWH. In summer, the lowest SWH occurs in the SCS, which may be accounted in two ways. The first explanation is that the wind speed in summer is dominated by the southwest monsoon, which is the smallest of the four seasons, basically around 6 m s^{-1}, as shown in Fig.7. The second reason is that the wave direction in summer is northward. In spring, autumn, and winter, waves propagate from the west Pacific into the SCS. The waves in the SCS are less affected by waves from the west Pacific Ocean in summer. So, with lower wind speed and fewer waves propagating from the west Pacific Ocean, the SWH in summer is lowest. Pressure from Mongolia is reinforced in autumn, and the enhanced northeast monsoon leads to a gradual increase in the SWH in the SCS. These results also indicate that spring and autumn are transition stages between the winter and summer monsoons.

The variation in the MWD in the Indian Ocean is relatively small and mainly northward. In the SCS, the MWD shows obvious seasonal variation. In spring and autumn, waves mainly propagate from the west Pacific Ocean to the SCS in a westerly direction. In summer, waves mainly propagate to the north. In winter, the waves propagate from the west Pacific Ocean to the south of the SCS with a high SWH.

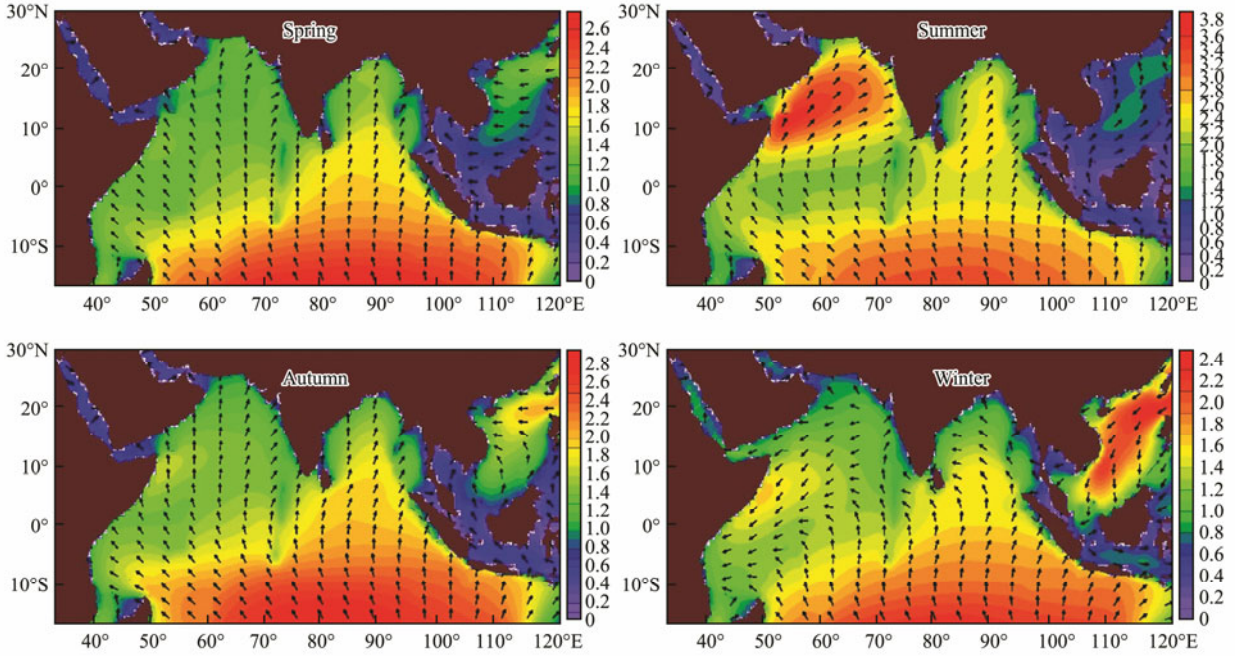

Fig.3 Seasonal-average distributions of SWH and MWD in different seasons. The black arrows indicate the MWD.

Fig.4 shows the annual-average distributions of SWH and MWD from 1979 to 2014. We can see that the SWH is relatively low in coastal areas and high in open seas. We find the highest SWH in the central Indian Ocean, and east of the Gulf of Aden, south of the Bay of Bengal, and the Luzon Strait in the SCS are also high-SWH regions. The waves in the Indian Ocean mainly propagate in the northerly direction. Waves in the SCS mainly propagate in a westerly direction from the west Pacific Ocean to the continent.

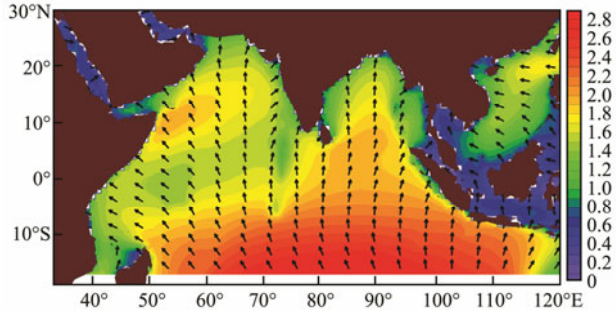

Fig.4 Annual-average distributions of SWH and MWD from 1979 to 2014. The black arrows indicate the MWD.

3.2 Distribution of the MWP

The MWP of swells usually exceeds 8 s, and low-frequency swells may pose threats to ships. Fig.5 shows the seasonal variations of the MWP, and we can see that the overall seasonal-average distribution in the study area is similar to the annual-average distribution of the MWP shown in Fig.6. The northwestern area of the North Indian Ocean shows obvious seasonal variation, whereas the eastern area shows a relatively stable MWP distribution. In the SCS, the MWP is small in spring and is smallest in summer due to the weak southwest monsoon. In autumn, the MWP begins to increase with the increasing monsoon, which gradually spreads to the south and becomes largest in winter. The MWP in the SCS decreases from the Luzon Strait to the Asian continental shelf, which can be explained by the swells from the west Pacific propagating through the Luzon Strait to the coastal areas (Nagai *et al*., 1998).

As shown in Fig.6, the annual-average distribution of the MWP shows obvious regional variations. The MWP of the North Indian Ocean is symmetrically longitudinal along the equator, with the maximum value at the equator. In the latitudinal direction, the distribution of the MWP is asymmetrical, with the larger MWP in the eastern area of the North Indian Ocean. The MWP is small in the western area, especially around the Arabian Sea and Gulf of Aden. The overall distribution of the MWP in the SCS is smaller than that in the North Indian Ocean, with largest value occurring in the Luzon Strait.

Based on Figs.5 and 6, we can see that the MWP in the central Indian Ocean usually exceeds 8 s, which indicates that it is swell-dominated in this area. This may be explained by the Roaring Forties westerly wind effect in the Southern Hemisphere, which also contributes to the SWH in the central Indian Ocean.

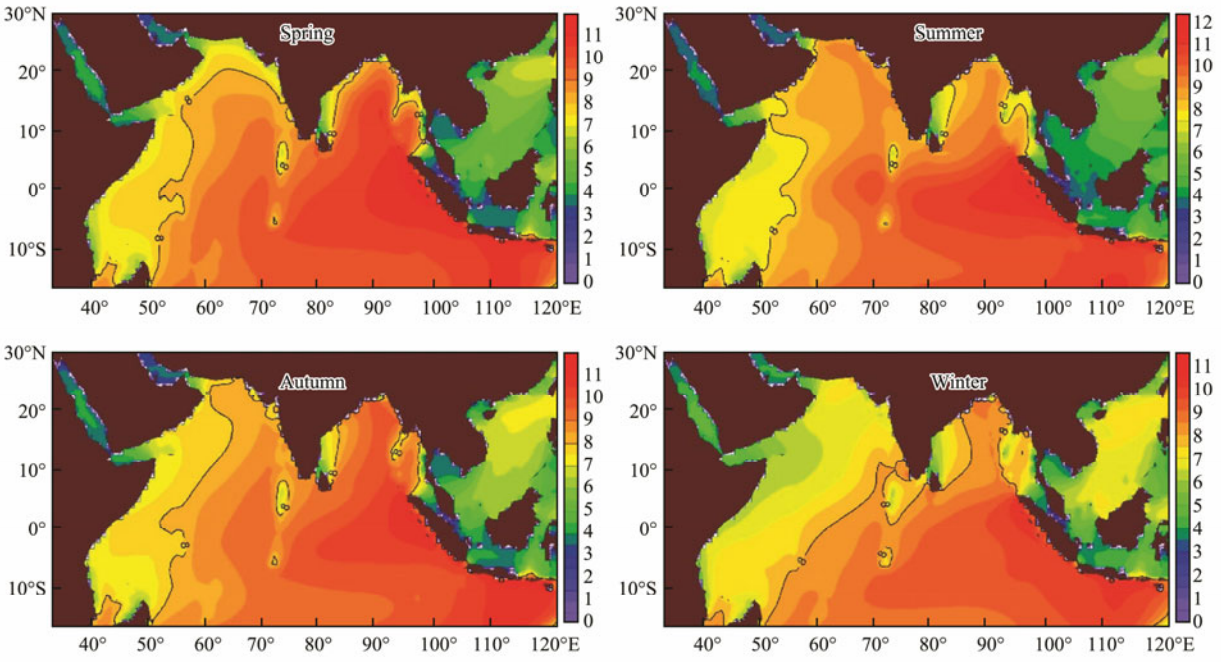

Fig.5 Seasonal-average distribution of the MWP in different seasons.

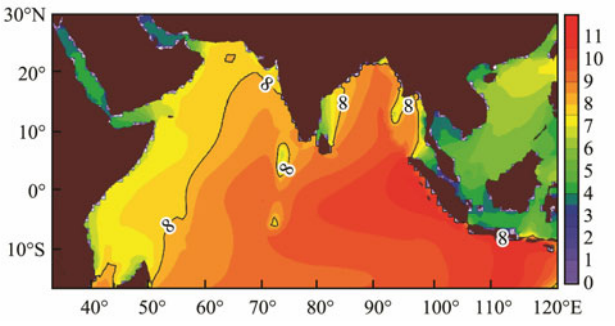

Fig.6 Annual-average distribution of the MWP from 1979 to 2014.

3.3 Distribution of the Wind Speed

The wind speed is greatly influenced by the seasons, and Fig.7 shows the seasonal distributions of the wind speed in the study area. Although the wind speed in the central Indian Ocean is mostly high and that along the equator is mostly low over the whole study area, seasonal variations do occur. The wind speed in the Bay of Bengal changes slightly in different seasons, generally by around 8 m s^{-1}. The wind speeds of the Gulf of Aden and SCS show obvious seasonal variations due to the effects of monsoon. In spring, the wind speed in the Gulf of Aden is

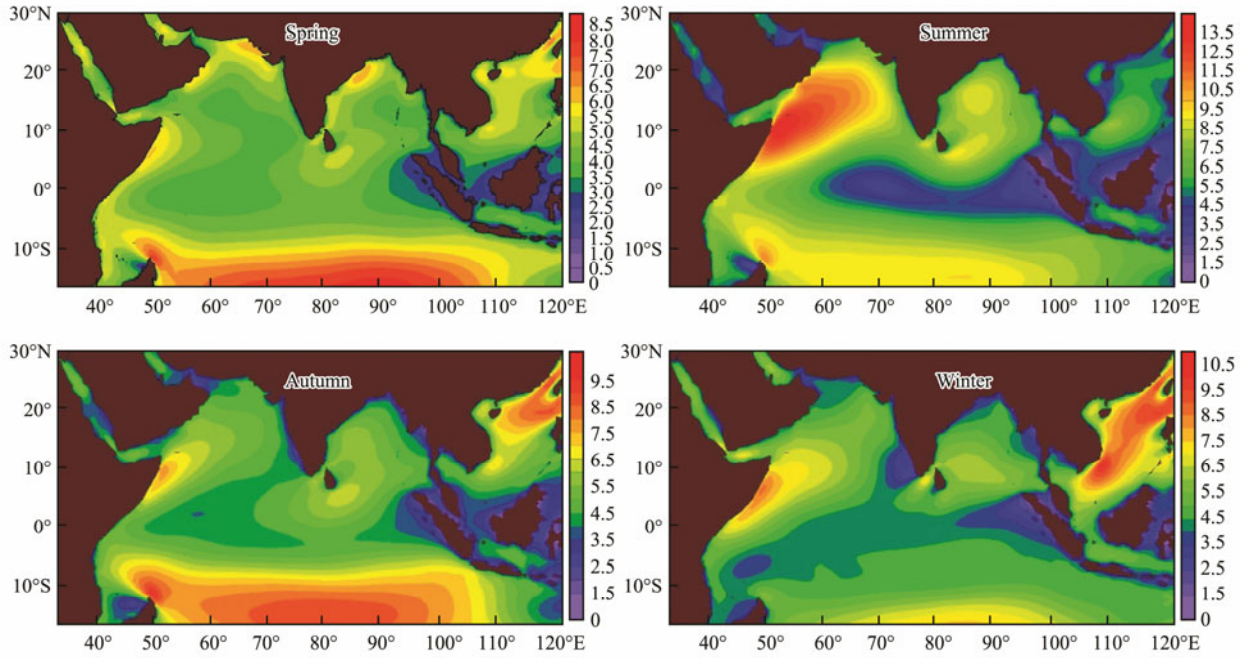

Fig.7 Seasonal-average distributions of wind speed in different seasons.

lowest and that in the North Indian Ocean is around 4 m s^{-1}. The wind speed in the SCS begins to decrease upon the weakening of the northeast monsoon. In summer, the wind speed in the Gulf of Aden is highest, whereas in the SCS it is lowest due to the weak southwest monsoon. In autumn, the northeast monsoon in the SCS begins to increase, which leads to increases in the wind speed (as shown in Fig.7) and SWH (as shown in Fig.3). The wind speed in the SCS increases gradually and is highest in winter.

As shown in Fig.8, the overall wind speed distribution is similar to the distribution of the SWH in Fig.4. Higher wind speeds appear in the east of the Gulf of Aden, the central Indian Ocean, and the Luzon Strait. The high-wind-speed regions are consistent with the high-SWH regions. The latitudinal distribution of the doldrums is obvious in both Figs.7 and 8.

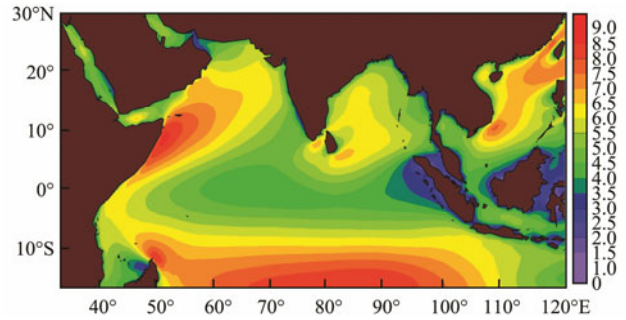

Fig.8 Annual-average distribution of wind speed from 1979 to 2014.

4 Discussion

Huge waves and high winds pose severe threats to ships, and the risks increase with higher SWHs and wind speeds. According to the Beaufort wind scale, an SWH of 4 m (huge waves) corresponds to a wind speed of 13.9 m s^{-1} (high winds). Here we first present the monthly and annual averages of huge waves and high winds. The results of our wave energy and wind energy analyses, which we present in this section, provide reference knowledge for ocean engineering purposes. In terms of energy, we explore SWH and wind speed to construct an RF as an indicator of navigation risk level. Finally, in this section, we analyze extreme weather conditions like cyclones to determine their impact on four major sea routes.

4.1 Distributions of Huge Waves and High Winds

We obtained the spatial distributions of the maximum wind speed and SWH in the study area for the period from 1979 to 2014, as shown in Figs.9 and 10.

In Fig.9, the wind speed in the SCS is higher and the extent of the high wind speed is broader, with the highest wind speed greater than 36 m s^{-1}. The Arabian Sea and Bay of Bengal also show two intensive regions of high wind speed, and we can see that the wind speed is low along the equator. Ocean waves with a SWH exceeding 4 m are considered to be huge waves. As shown in Fig.9, the maximum wind speed for most regions exceeds 13.9 m s^{-1}, which indicates terrible sea conditions.

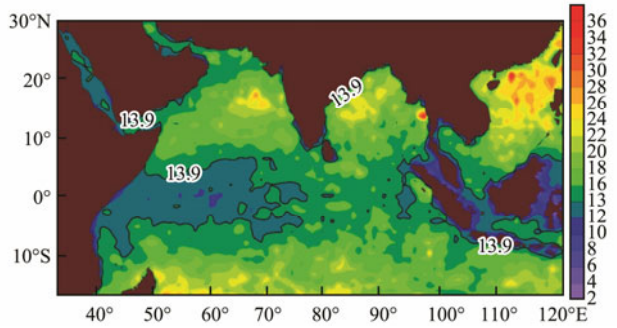

Fig.9 Spatial distribution of maximum wind speed in the study area from 1979 to 2014. The black solid line contour indicates a wind speed of 13.9 m s^{-1}.

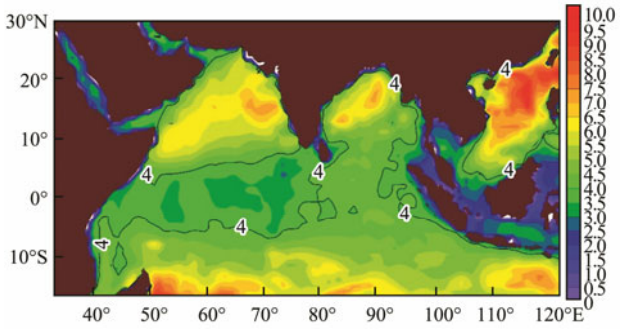

Fig.10 Spatial distribution of maximum SWH in the study area from 1979 to 2014. The black solid line contour indicates an SWH of 4 m.

The distribution characteristics of Figs.9 and 10 are similar. In Fig.10, the highest SWH in most regions of the study area reaches the classification threshold for huge waves (SWH > 4 m). Moreover, the SWH of most regions in the SCS exceeds 7 m, with the highest SWH reaching 10 m. The highest SWHs in most regions of the Arabian Sea, Bay of Bengal, and the central Indian Ocean also exceed 6 m. From Figs.9 and 10, we can conclude that the maximum wind speed and SWH in most regions of the study area guarantee the existence of dangerous sea conditions. As such, it is necessary to conduct a more detailed analysis of the SWH and wind speed to gain a more comprehensive understanding of the sea conditions in the study area.

Figs.11 and 12 show the distributions of the monthly average frequencies for huge waves and high winds, respectively.

As shown in Fig.11, from March to May the overall wind speed is relatively low, with almost no high wind occurring, especially in April. In spring, the lowest occurrence frequency of high wind (just 1%) occurs in the Luzon Strait during March. However, from June to August the sea conditions begin to worsen, with the seasonal-average frequency of high wind reaching 56%. In July, the highest frequency of high wind speed occurs, reaching a surprising 80%, mainly in the eastern regions

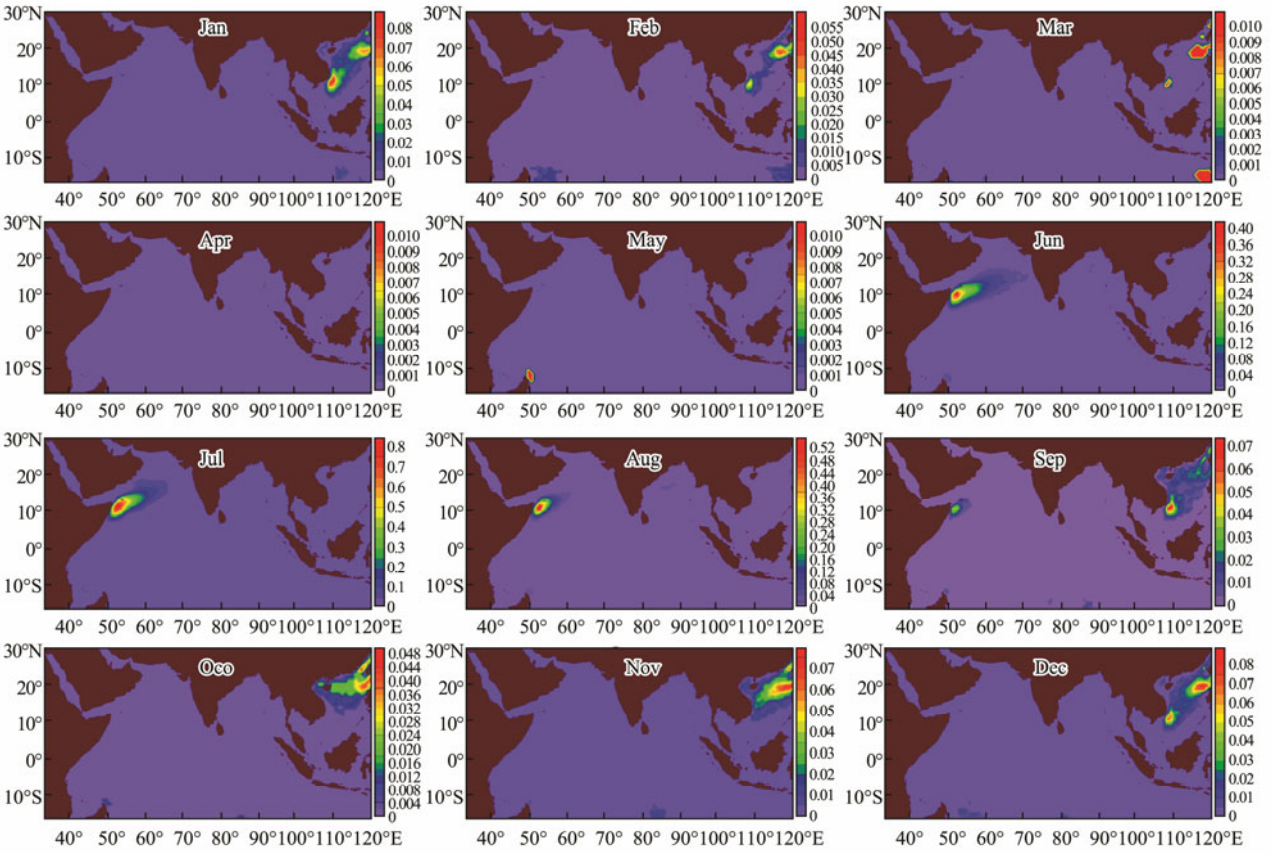

Fig.11 Distributions of monthly average frequency for wind speeds exceeding 13.9 m s^{-1}. The twelve months from January to December are arranged from up to down and left to right.

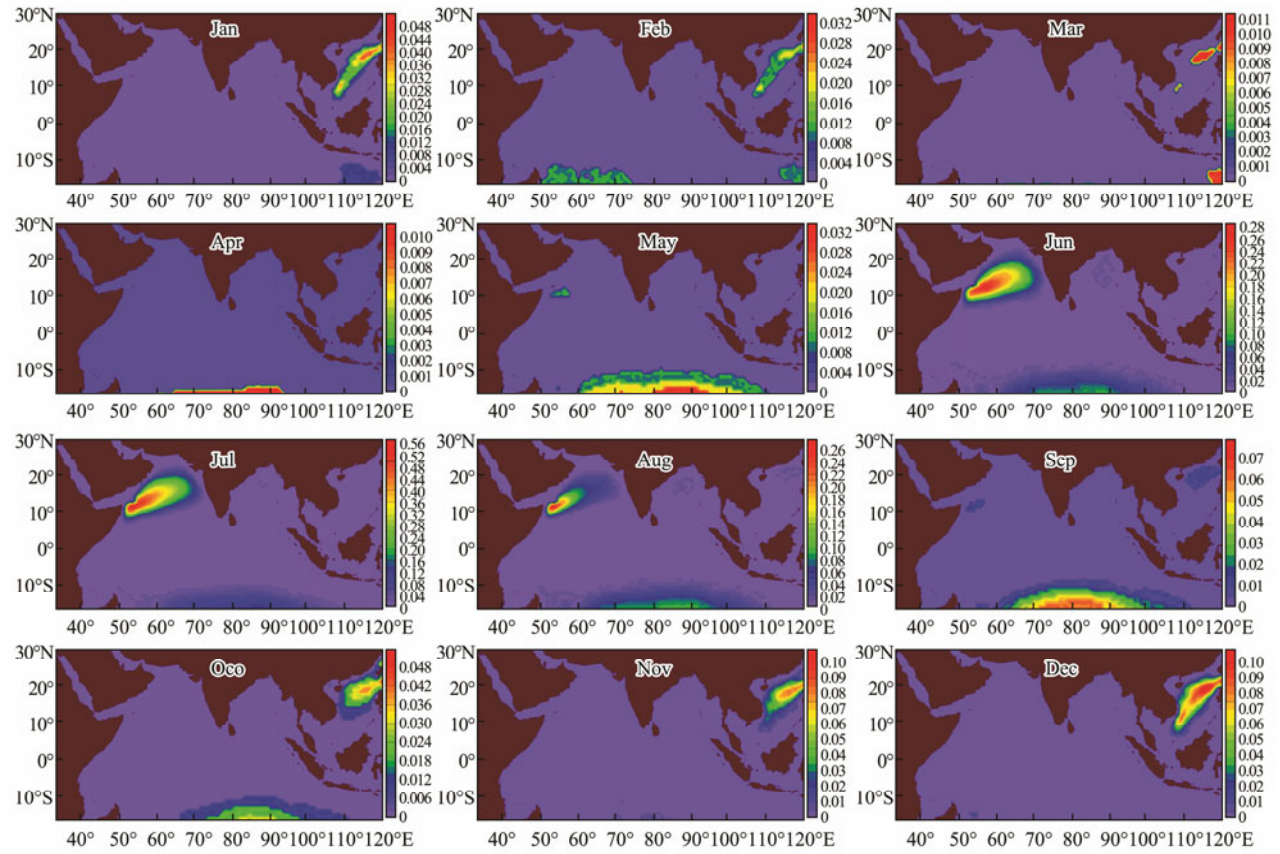

Fig.12 Distribution of monthly average frequency of the SWH exceeding 4 m. The twelve months from January to December are arranged from up to down and left to right.

of the Gulf of Aden, which indicate terrible sea conditions in summer. In contrast, due to the weak southwest monsoon, no high wind occurs in the SCS. From September to November, almost no high wind occurs in the North Indian Ocean, apart from the fading effect of the 'strong summer' in the Gulf of Aden, where it reaches 3% in September. However, the wind speed in the SCS begins to increase, with the highest frequency reaching 7% in the Luzon Strait. In winter, the wind speed in the SCS is highest with broad coverage due to the strong northeast monsoon. The wind speed of the SCS begins to fade in February of the following year.

The distributions shown in Fig.12 are similar to those in Fig.11 in most regions. In July, the occurrence frequency of high wind speed for regions east of the Gulf of Aden is 80% (Fig.11) and correspondingly the occurrence frequency of huge waves (SWH>4 m) reaches 56%. For the whole summer, the seasonal-average frequencies of high wind speed and huge waves are 56% and 36%, respectively. These high frequencies indicate terrible sea conditions for regions east of the Gulf of Aden. In summer, ships traveling through this region will face severe threat. In December, the occurrence frequency of huge waves in the SCS reaches its annual high, which is also the case for high wind. This means that the sea conditions of the SCS in winter are also terrible. Overall, in Figs.11 and 12, the SCS is safe for maritime travel in summer and the North Indian Ocean is relatively safe in winter.

Although Figs.11 and 12 share similarities in their distributions, we found discrepancies in the central Indian Ocean. In Fig.11, we can see that almost no high wind speed occurs in the central Indian Ocean, but from April to October, we can see huge waves in the central Indian Ocean in Fig.12, up to 10%. This discrepancy indicates that the huge waves frequently occurring in the central Indian Ocean are not induced by high wind speed, which proves again that the high SWH (see Fig.4) is the effect of swell propagating from the Southern Ocean.

4.2 Distributions of the Wave and Wind Energies

Wave energy and wind energy are attractive renewable energies with large reserves and wide distributions. Figs.13 and 14 show the distributions of wave energy and wind energy, respectively, in different regions of the study area. From the seasonal-average distribution, we see that the wave energy in the SCS shows obvious seasonal variation, with the highest value appearing in winter, which then decreases gradually from the Luzon Strait to the coast. For the North Indian Ocean, the Gulf of Aden shows the highest value in summer but low values in the other seasons. The wave energy is highest in the central Indian Ocean in every season, which indicates good stability.

We found almost no stable wind-energy regions in the study area. The Gulf of Aden and the Luzon Strait continue to show obvious seasonal variations, and the central Indian Ocean shows a low energy distribution in summer and winter. Note that the wind energy in the Gulf of Aden is extremely high in summer, up to 1800 W m^{-2}.

4.3 Distributions of Risk Factors

In calculations of wave and wind energies, wind speed and SWH are key factors. Higher wind speeds and SWHs correspond to higher energy. High wind speeds and high SWHs threaten navigation security. To analyze the combined effect of wind and waves, we propose the RF measure for evaluating navigation safety levels. The RF is a product of SWH and wind speed, and we normalize the RF as follows:

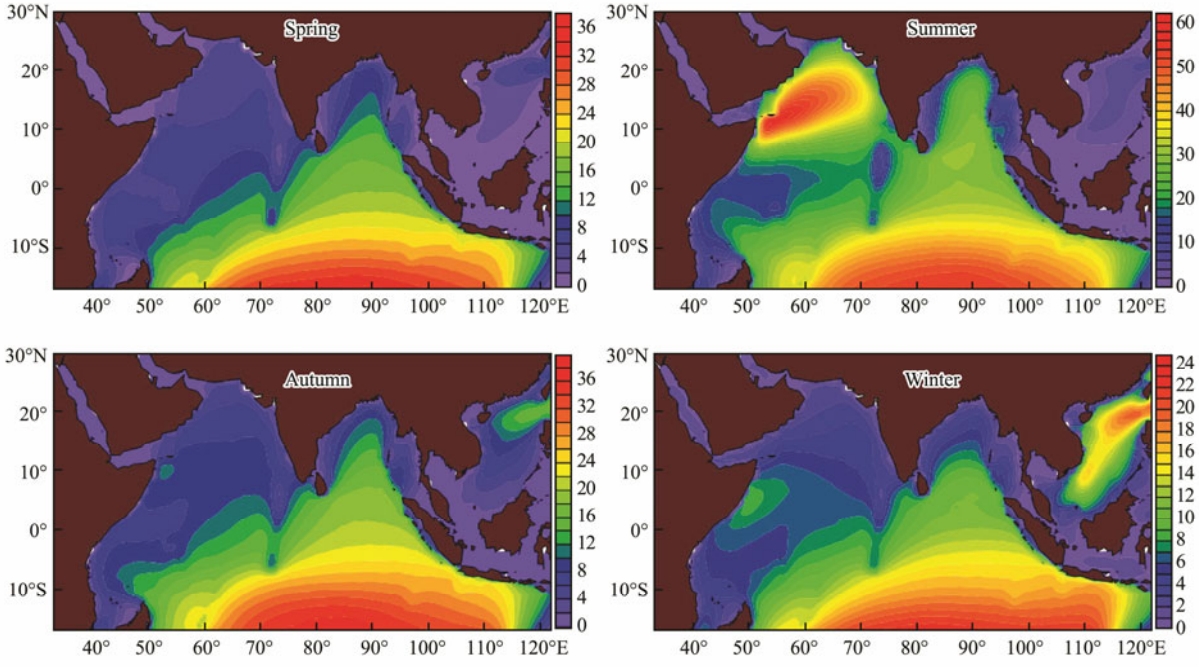

Fig.13 Distributions of wave energy in different seasons.

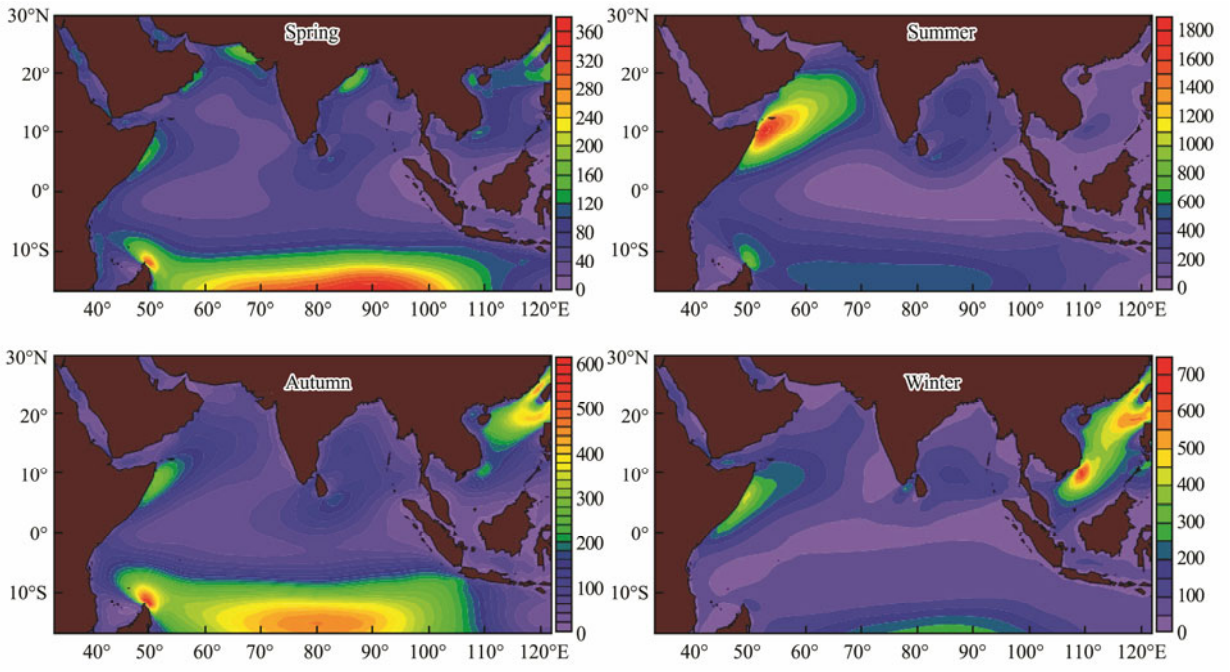

Fig.14 Distributions of wind energy in different seasons.

$$RF = \frac{SWH \cdot WindSpeed}{\max(SWH \cdot WindSpeed)}.$$

When $RF=1$, this indicates the most dangerous conditions in the study area. In this section, we discuss the impact of RF on the MSR and three other major sea routes in the study area. The results of our previous analyses indicate that the wind speed and SWH undergo obvious seasonal variations, and Fig.15 shows the seasonal RF distributions.

In Fig.15, the black dotted line (Route 1) represents the route of the 21st MSR and the gray dotted lines (Routes 2, 3, 4) represent portions of three other major sea routes through the study area. Route 2 is the sea route connecting Asia and Europe through the Suez Canal, which significantly shortens the voyage. Route 3 is the ship sea route from South Africa's Cape of Good Hope to harbors in Asia, which is known by many countries as the maritime lifeline. Large ships that cannot travel through the Suez Canal do so around the Cape of Good Hope. Most oil transport occurs along this route. Route 4 is the sea route between Calcutta and Oceania.

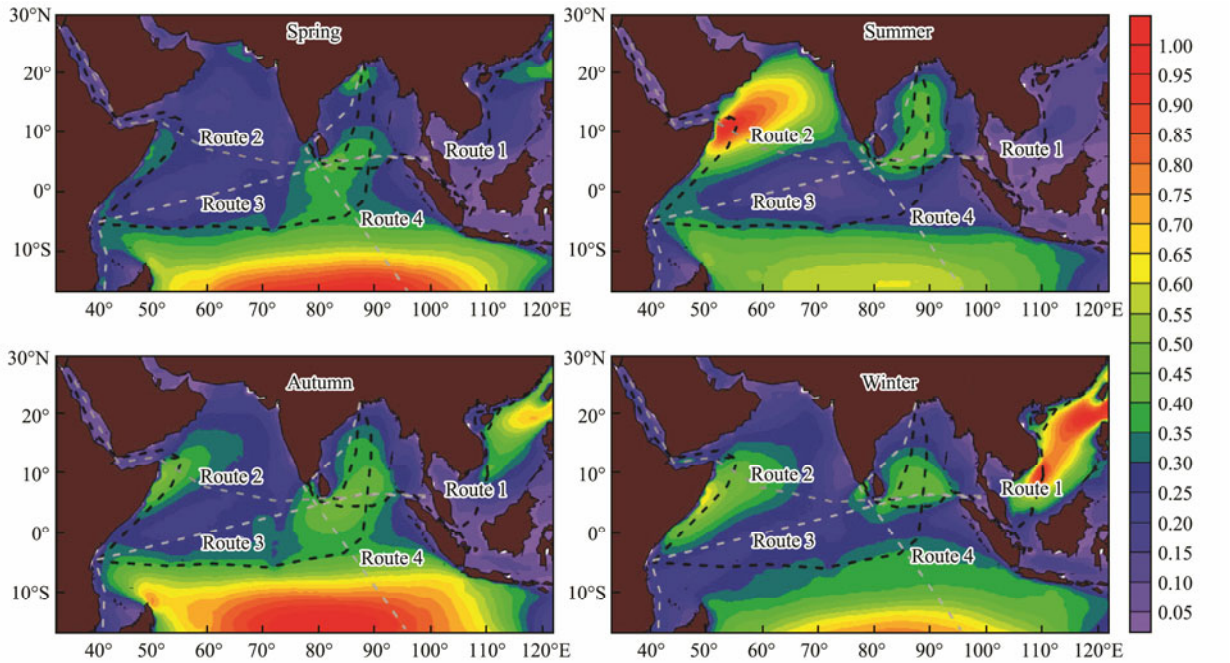

Fig.15 Seasonal *RF* distributions in the study area. The black dotted line represents the MSR and other three gray dotted lines represent three other major sea routes.

As shown in Fig.15, in spring the RF in the SCS and North Indian Ocean is low, around 0.2, so Routes 1, 2, and 3 are suitable for maritime travel. However, the *RF* in the central Indian Ocean can reach 0.8, which makes it dangerous for Route 4. In summer, the RFs in the SCS and the Bay of Bengal are relatively low and that of central Indian Ocean is also decreased. High RFs occur in the east of the Gulf of Aden, which means terrible sea conditions. As mentioned above, in summer high winds and huge waves frequently occur in the Gulf of Aden, thus greatly affecting Routes 1 and 2 in this region. Route 4 is suitable for maritime travel in summer, showing a lower RF in the central Indian Ocean. In autumn, high RF in the SCS begins to spread southwest from the Luzon Strait, and in the central Indian Ocean high RF values begin to spread northward, which means increasingly dangerous sea conditions. Ships traveling along Route 1 are at the edges of the dangerous regions in both the SCS and central Indian Ocean. Route 4 is significantly affected in the central Indian Ocean during this time. Meanwhile, we note that the RF in the Gulf of Aden begins to decrease. In winter, the SCS is the most dangerous region for maritime travel, with the RF in most regions exceeding 0.7, whereas the RF in the North Indian Ocean is relatively low. In general, Route 1 is suitable for ship travel in summer; Route 2 is safest in spring and most dangerous in summer; Route 3 goes through the doldrums region and is safe throughout the year, although it may be affected to some extent in autumn; and Route 4 is mainly affected by the swell in the central Indian Ocean, which is dangerous in spring and autumn.

4.4 Distributions of Tropical Cyclones

Tropical cyclones will induce strong winds and huge waves, which can severely threaten ship navigation. In this section, we analyze the spatial distribution of tropical cyclones in the study area from 2000 to 2015, as shown in Fig.16. Our major focus is on the sea influence, so the tropical cyclone tracks over land are covered by the base map.

The tropical cyclones over the study period are mainly distributed in regions located 10 degrees away from the equator. Globally, the west Pacific experiences the most tropical cyclones, which travel westward and cover almost the entire SCS. Tropical cyclones in the SCS mainly occur from May to December, with fewer cyclones observed in winter (Wang *et al*., 2009). In the North Indian Ocean, the Bay of Bengal is greatly affected by tropical cyclones, whereas the Arabian Sea is only relatively weakly affected. In terms of occurrence time, tropical cyclones in the North Indian Ocean show 'double peaks' in May, June and November, December (Gray, 1968). The southern Indian Ocean is also greatly affected by tropical cyclones, which mainly occur from December to March of the following year (Ho *et al*., 2006).

Almost all of Route 1 is affected by tropical cyclones in the SCS and the Bay of Bengal. Regions between Vietnam and Malaysia, the Java Sea, and the Strait of Malacca are less affected. Ships traveling along Route 1 are in the intensive tropical cyclones regions of the North Indian Ocean. Routes 2 and 3 are mainly along the equator, so they are less influenced by tropical cyclones. Route 4 is mainly affected in the Bay of Bengal and central Indian Ocean. Based on the above analysis, in regions prone to tropical cyclones, ships traveling along the four routes should pay close attention to forecasts to avoid tropical cyclones.

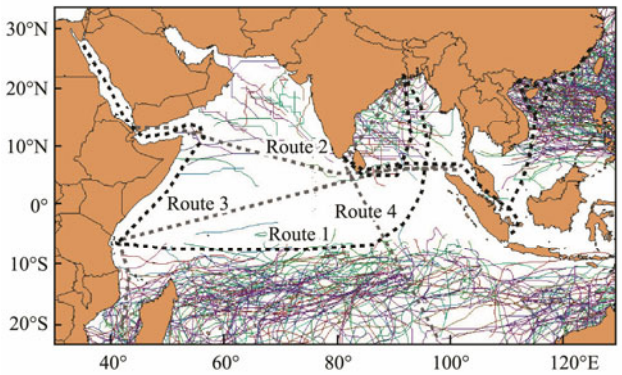

Fig.16 Spatial distribution of tropical cyclones in the study area. The colored solid lines indicate the best tracks of tropical cyclones and the different colors represent different years.

5 Conclusions

In this paper, we presented the spatial and temporal distributions of wind speed, MWD, SWH, and MWP of ocean waves in the MSR for the period from 1979 to 2014. We analyzed the occurrence frequencies of high winds and huge waves in the study area. We also briefly discussed the distributions of wave energy and wind energy to provide references for ocean engineering purposes. The analysis results indicate that the Luzon Strait and Gulf of Aden experience the most obvious seasonal variations.

We proposed the calculation of an RF for evaluating the navigation safety level of ships and we also presented the seasonal RF distributions. This analysis showed that, in spring, Routes 1, 2, and 3 are suitable for maritime travel in the SCS and North Indian Ocean; in summer, the SCS and Bay of Bengal are relatively safe but the RF in the Gulf of Aden is extremely high, with the highest occurrence frequencies of high wind speed and huge waves being 80% and 56%, respectively; in autumn, the RF in the SCS begins to spread southwest from the Luzon Strait and that in the central Indian Ocean begins to spread northward, which will affect ships traveling along Routes 1 and 4; in winter, the SCS has the highest RF, reaching 0.7, and the RF in the North Indian Ocean is relatively low. Due to effect of the doldrums, the RF along the equator remains low in every season.

We extracted the best tracks of tropical cyclones from the IBTrACS for the period from 2000 to 2015 and presented their spatial distribution in the study area. We found that Route 1 is affected by tropical cyclones mainly in the SCS and Bay of Bengal. Routes 2 and 3 are less affected because of their along-the-equator distribution

characteristic. Route 4 is affected mainly in the Bay of Bengal and central Indian Ocean. We analyzed the frequent occurrence time of tropical cyclones for different regions. In conclusion, our analysis of the dynamic characteristics (wind, wave, and tropical cyclone) of the 21st MSR and their effect on sea routes provide references for the security of ship navigation as well as ocean engineering.

Acknowledgements

The authors would like to thank the ECMWF for providing the ERA-Interim dataset. This work is supported by the National Key R&D Program of China under contract No. 2016YFC1402703 and the National Youth Natural Science Foundation under contract No. 61501130. The work is also supported by the Fundamental Research Funds for the Central Universities under contract No. 16CX02033A. The best tracks of tropical cyclones were downloaded from the International Best Track Archive for Climate Stewardship (http://www.ncdc.noaa.gov/ibtracs/index.php?name=ibtracs-data-access).

References

Anoop, T. R., Kumar, V. S., Shanas, P. R., and Johnson, G., 2015. Surface wave climatology and its variability in the North Indian Ocean based on ERA-interim reanalysis. *Journal of Atmospheric & Oceanic Technology*, **32**: 1372-1385.

Bhat, G. S., and Fernando, H. J., 2016. Remotely driven anomalous sea-air heat flux over the North Indian Ocean during the summer monsoon season. *Oceanography*, **29** (2): 232-241.

Chu, P. C., and Cheng, K. F., 2008. South China Sea wave characteristics during typhoon Muifa passage in winter 2004. *Journal of Oceanography*, **64** (1): 1-21.

Gray, W. M., 1968. Global view of the origin of tropical disturbances and storms. *Monthly Weather Review*, **96**: 669-700.

Ho, C. H., Kim, J. H., Jepng, J. H., Kim, H. S., and Chen, D., 2006. Variation of tropical cyclone activity in the South Indian Ocean: El Niño-Southern Oscillation and Madden-Julian Oscillation effects. *Journal of Geophysical Research Atmospheres*, **111**: D22101.

Jignesh, K., Abhijit, S., and Raj, K., 2001. Comparison of TOPEX/POSEIDON altimeter derived wind speed and wave parameters with ocean buoy data in the North Indian Ocean. *Marine Geodesy*, **24** (3): 131-138.

Liu, B. Q., Zhu, C. W., Yuan, Y., and Xu, K., 2016. Two types of interannual variability of South China Sea summer monsoon onset related to the SST anomalies before and after 1993/94. *Journal of Climate*, **29** (19): 6957-6971.

Liu, T. J., Zheng, C. W., Li, X. Q., and Zhang, W. J., 2013. Long term trend of sea surface wind speed in the northern Indian Ocean from 1958 to 2001. *Marine Forecasts*, **30** (4): 34-39 (in Chinese with English abstract).

Luo, M., Leung, Y., Graf, H. F., Herzog, M., and Zhang, W., 2016. Interannual variability of the onset of the South China Sea summer monsoon. *International Journal of Climatology*, **36** (2): 550-562.

Lv, X., Yuan, D., Ma, X., and Tao, J., 2014. Wave characteristics analysis in Bohai Sea based on ECMWF wind field. *Ocean Engineering*, **91**: 159-171.

Mei, Y., Song, S., and Zhou, L., 2010. Interdecadal variations of sea surface wind and significant wave height in the North Indian Ocean and South China Sea. *Marine Forecasts*, **34** (5): 27-33 (in Chinese with English abstract).

Murakami, H., Sugi, M., and Kitoh, A., 2012. Future changes in tropical cyclone activity in the North Indian Ocean projected by high-resolution MRI-AGCMs. *Climate Dynamics*, **40** (7-8): 1949-1968.

Nagai, K., Kono, S., and Quang, D. X., 1998. Wave characteristics on the central coast of Vietnam in the South China Sea. *Coastal Engineering Journal*, **40** (4): 347-366.

Ng, E. K. W., and Chan, J. C. L., 2012. Interannual variations of tropical cyclone activity over the North Indian Ocean. *International Journal of Climatology*, **32** (6): 819-830.

Qi, P., and Cao, L., 2016. The assimilation of Jason-2 significant wave height data in the North Indian Ocean using the ensemble optimal interpolation. *IEEE Transactions on Geoscience and Remote Sensing*, **54** (1): 287-297.

Rajasree, V. P. M., Kesarkar, A. P., Bhate, J. N., Singh, V., Umakanth, U., and Varma, T. H., 2016. A comparative study on the genesis of North Indian Ocean tropical cyclone Madi (2013) and Atlantic Ocean tropical cyclone Florence (2006). *Journal of Geophysical Research: Atmospheres*, **121** (13): 826-858.

Sabique, L., Annapurnaiah, K., Nair, T. M. B., and Srinivas, K., 2012. Contribution of southern Indian Ocean swells on the wave heights in the northern Indian Ocean □ A modeling study. *Ocean Engineering*, **43** (2): 113-120.

Sabique, L., Nair, T. M. B., Srinivas, K., and Nayak, N. S., 2013. Comparison of grid averaged altimeter and buoy significant wave heights in the northern Indian Ocean. *Marine Geodesy*, **36** (1): 72-85.

Semedo, A., Sušelj, K., Rutgersson, A., and Sterl, A., 2011. A global view on the wind sea and swell climate and variability from ERA-40. *Journal of Climate*, **24** (5): 1461-1479.

Shanas, P. R., and Sanil, K. V., 2014. Temporal variations in the wind and wave climate at a location in the eastern Arabian Sea based on ERA-Interim reanalysis data. *Natural Hazards & Earth System Sciences*, **14** (5): 7239-7269.

Wang, G., Ling, Z., and Wang, C., 2009. Influence of tropical cyclones on seasonal ocean circulation in the South China Sea. *Journal of Geophysical Research Oceans*, **114**: C10022.

Werner, A., Maharaj, A. M., and Holbrook, N. J., 2012. A new method for extracting the Enso-independent Indian Ocean dipole: Application to Australian region tropical cyclone counts. *Climate Dynamics*, **38** (11-12): 2503-2511.

Yuan, J., Wang, D., Liu, C., Han, H., and Huang, H., 2007. The characteristic differences of tropical cyclones forming over the western North Pacific and the South China Sea. *Acta Oceanologica Sinica*, **26** (4): 29-43.

Zheng, C. W., Pan, J., and Li, J. X., 2013. Assessing the China Sea wind energy and wave energy resources from 1988 to 2009. *Ocean Engineering*, **65** (2): 39-48.

Zheng, C. W., Pan, J., Sun, W., Chen, X., and Xia, L. L., 2015. Study on marine environment characteristics of 21st century Sea Silk Road. *Ocean Development and Management*, **7**: 4-9 (in Chinese with English abstract).

(Edited by Xie Jun)